

Development prospects and stability limits of the mid-IR Kerr-lens mode-locked lasers

V.L. Kalashnikov, E. Sorokin, and I.T. Sorokina

Institut für Photonik, TU Wien, Gusshausstr. 27/387, A-1040 Vienna, Austria

ABSTRACT

The Kerr-lens mode locking ability and the ultrashort pulse characteristics are analyzed numerically for the Cr-doped ZnTe, ZnSe, ZnS active media. The advantages of these materials for the femtosecond lasing within 2 - 3 μm spectral range are demonstrated.

Keywords: ultrashort pulses, Kerr-lens mode-locking, mid-infrared solid-state lasers, Cr-doped Zinc-chalcogenides

1. INTRODUCTION

Compact diode-pumped sources of the femtosecond pulses tunable within the wavelength range between 2 and 3 μm are of interest for various applications, such as laser surgery, remote sensing and monitoring, spectroscopy of semiconductors etc. To date only cryogenically operated Pb-salt diode lasers, optical parametrical oscillators and difference-frequency convertors were available for the operation in this spectral range. Therefore the possibility of the direct mid-IR lasing from the new class of the transition-metal doped chalcogenides^{1,2,3,4} has attracted much attention. The impressive advantages of these media are room-temperature operation between 2 and 3 μm , possibility of direct diode pumping, high emission and absorption cross-sections, negligibly low excited-state absorption and, as consequence, low thermal load (the basic laser material characteristics will be described in the next section). The most remarkable examples of such lasers are Cr²⁺-doped ZnSe, ZnS and ZnTe. To date the following achievements for these media have been demonstrated: 1) for Cr:ZnSe CW operation with over 1.7 W power,⁵ over 1100 nm tunability,⁶ over 350 nm tunable diode-pumped CW operation,⁷ active mode locking⁸ and active modulator assisted passive mode locking⁹ were achieved; 2) for Cr:ZnS pulsed^{2,10} and tunable CW operation¹¹ were obtained. Cr:ZnTe, which is a member of the considered media class, remains unexplored.

In spite of the numerous advantages, there exist some obstacles for femtosecond pulse generation from these lasers. As they are the semiconductors, i.e. possess a comparatively narrow band-gap, the nonlinear refraction in the active crystal is large (see below). Hence the self-focusing has a comparatively low threshold which in the combination with the self-phase modulation produce a tendency to the multiple pulse operation in the Kerr-lens mode locking (KLM) regime.^{9,12} Thus, there is a need in the study of the KLM stability limits and methods of the stability enhancement in the considered lasers. Moreover, the large absorption and emission cross sections tend to the stabilization of the CW operation, which prevents the KLM self-start.

In this paper we present an analysis of the nonlinear refraction in the Zinc-chalcogenides (by the example of ZnSe). In the combination with the lasing properties this defines the main requirements to the KLM optimization. Then, the results of the numerical optimization of the KLM aimed at the multipulsing suppression and taking into account a strong saturation of the Kerr-lens induced fast absorber are presented. We demonstrate the possibility of the few optical cycle pulse generation from the Cr-doped Zinc-chalcogenodes. The problem of the self-starting KLM is analyzed on the basis of the generalized momentum method taking into account real-world laser configurations, gain guiding, soft-aperture, thermo-lensing and other properties of the considered laser materials. The presented models are quite general and can be applied to the overall optimization of the different KLM lasers.

Further author information: (Send correspondence to Dr. V.L. Kalashnikov)
V.L. Kalashnikov: E-mail: v.kalashnikov@tuwien.ac.at

2. DISTRIBUTED MODEL AND BASIC PARAMETERS

Simulation of the KLM can be based on the two quite different approaches. First one supposes the full-dimensional modelling taking into account the details of the field propagation in the laser cavity.¹³ The minimal dimension of such models is 2+1 and they allow the description of the spatio-temporal dynamics of the ultrashort pulses and their mode pattern. Its main disadvantages are a large number of the parameters resulting in ambiguity of the optimization procedure and complexity of the interpretation of the obtained results. Second approach is based on 1+1 dimensional model in the framework of the so-called nonlinear Ginzburg-Landau equation,¹⁴ which describes the KLM as an action of the fast saturable absorber governed by the few physically meaningful parameters, viz., its modulation depth γ and the inverse saturation intensity σ . This method allows the analytical realization in the weak-nonlinear limit,¹⁵ however in the general case the numerical simulations are necessary. We shall base our analysis on the both approaches.

In the beginning let us consider the master equation describing the ultrashort pulse generation in the KLM solid-state laser:

$$\frac{\partial a(z, t)}{\partial z} = \left[\alpha - \rho + \left(t_f^2 \frac{\partial^2}{\partial t^2} - i \sum_{m=2}^N \frac{(-i)^m \beta_m}{m!} \frac{\partial^m}{\partial t^m} \right) - \frac{\gamma}{1 + \sigma |a(z, t)|^2} - i\delta \left(|a(z, t)|^2 - \frac{i}{\omega_0} \frac{\partial}{\partial t} |a(z, t)|^2 \right) \right] a(z, t), \quad (1)$$

where $a(z, t)$ is the field amplitude (so that $|a|^2$ has a dimension of the intensity), z is the longitudinal coordinate normalized to the cavity length (thus, as a matter of fact, this is the cavity round-trip number), t is the local time, α is the saturated gain coefficient, ρ is the linear net-loss coefficient taking into account the intracavity and output losses, t_f is the group delay caused by the spectral filtering within the cavity, β_m are the m -order group-delay dispersion (GDD) coefficients, $\delta = l_g n_2 \omega_0 / c = 2\pi n_2 l_g / (\lambda_0 n)$ is the self-phase modulation (SPM) coefficient, ω_0 and λ_0 are the frequency and wavelength corresponding to the gain band maximum, n and n_2 are the linear and nonlinear refraction indexes, respectively, l_g is the double length of the gain medium (we suppose that the gain medium gives a main contribution to the SPM). The last term in Eq. (1) describes the self-steepening effect and for the simplification will be not taken into account in the simulations. As an additional simplification we neglect the stimulated Raman scattering in the active medium.¹⁶ These two factors will be considered hereafter.

The gain coefficient obeys the following equation:

$$\frac{\partial \alpha(z, t)}{\partial t} = \sigma_a (\alpha_{\max} - \alpha(z, t)) \frac{I_p}{\hbar \omega_p} - \sigma_g \alpha(z, t) \frac{|a(z, t)|^2}{\hbar \omega_0} - \frac{\alpha(z, t)}{T_r}. \quad (2)$$

Here σ_a and σ_g are the absorption and emission cross-sections of the active medium, respectively, T_r is the gain relaxation time, I_p is the absorbed pump intensity, ω_p is the pump frequency, $\alpha_{\max} = \sigma_g N_g l_g$ is the maximum gain coefficient, N_g is the concentration of the active centers. The assumption $\tau_p \ll T_{cav}$ (τ_p is the pulse duration, T_{cav} is the cavity period) allows the integration of Eq. (2). Then for the steady-state gain coefficient we have:

$$\alpha = \frac{\alpha_{\max} \sigma_a I_p T_{cav}}{\hbar \omega_p \left(\frac{\sigma_a I_p T_{cav}}{\hbar \omega_p} + \frac{E}{E_s} + \frac{T_{cav}}{T_r} \right)}, \quad (3)$$

where $E_s = \hbar \omega_p / \sigma_g$ is the gain saturation energy flux, $E = \int_{-T_{cav}/2}^{T_{cav}/2} |a(t)|^2 dt$ is the pulse energy.

For the numerical simulations in the framework of the distributed model it is convenient to normalize the time and the intensity to $t_f = \lambda_0^2 / (\Delta \lambda c)$ and $1/\delta$, respectively ($\Delta \lambda$ is the gain bandwidth). The simulation were performed on the $2^{12} \times 10^4$ mesh. Only steady-state pulses were considered. As the criterion of the steady-state operation we chose the peak intensity change less than 1% over last 1000 cavity transits.

The KLM in the considered model (1, 3) is governed by the only four basic parameters: $\alpha - \rho$, β_2 , γ , and σ . This allows unambiguous multiparametric optimization. In the presence of the higher-order dispersions, the additional β_m parameters appear. This complicates the optimization procedure, but keeps its physical clarity.

Now let us consider the basic active media parameters.

Table 1. Material parameters of the Cr-doped Zinc-chalcogenides.

Medium	λ_0 , μm	$\Delta\lambda$, nm	λ_a , μm	σ_a , 10^{-19} cm ²	σ_g , 10^{-19} cm ²	n	n_2 , 10^{-13} esu	T_r , μs
Cr:ZnSe	2.5	880	1.61	8.7	9	2.44	29 – 92	6-8
Cr:ZnS	2.35	800	1.61	5.2	7.5	2.3	16 – 30	4-11
Cr:ZnTe	2.6	800	1.61	12	20	2.71	80 – 150	3

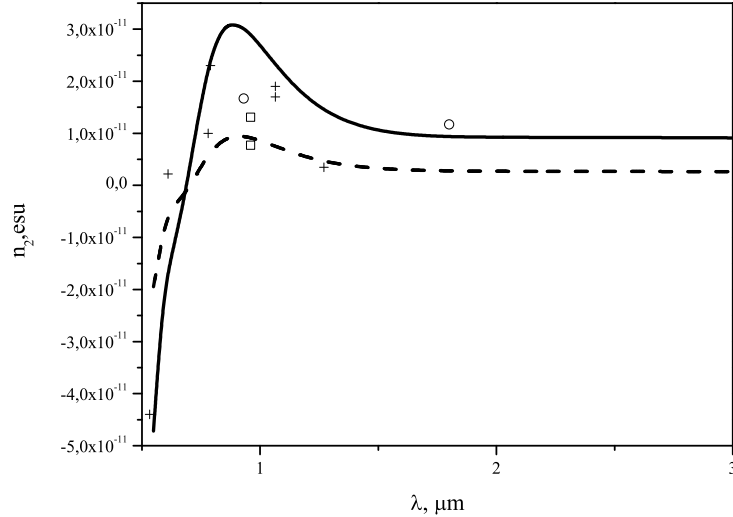


Figure 1. Calculated wavelength dependence of n_2 for ZnSe. Solid and dashed curves present the maximum and minimum estimations based on Eq. (4). Points give the experimental data for polycrystalline samples, squares – for monocrystals with different orientations, crosses – unknown crystalline structures.

It should be noted that the n_2 values were experimentally measured at the wavelengths which are smaller than λ_0 (see Fig. 1). Therefore we have to estimate theirs at the generation wavelength. Such estimation can be obtained from the two¹⁷ or four¹⁸ bands models of semiconductor. The most simple estimation results from the former model, which gives the following formula:

$$n_2(esu) = K \frac{G(\hbar\omega/E_g)\sqrt{E_p}}{nE_g^4}, \quad (4)$$

where $K = (0.5 - 1.5) \times 10^{-8}$ and $E_p = 21$ eV are the material independent constants, E_g is the band-gap width in eV, G is the form-factor. Using for K the values $0.86 - 1.5 \times 10^{-8}$ and for E_p the values 21–24 eV, we obtained the estimations presented in Table 1. The calculated n_2 dispersion for ZnSe is shown in Fig. 1.¹⁹

We note that the semiconductor nature of these active media results in the extremely high nonlinear refraction coefficients in the comparison with Ti:sapphire (1.2×10^{-13} esu). Also, we have to note that there exists the orientational dependence of n_2 , which can be especially large for the birefringent ZnS. But even for the cubic ZnSe, the orientational variation of n_2 can reach 70% (see Fig. 2).

In addition to the large n_2 the considered media possess the strong quadratic-nonlinearity due to absence of the center of inversion (for ZnSe and ZnTe). For example, $d_{36} = 33$ pm/V for ZnSe. However, as a result of the cubic structure, there exists the strong orientational dependence of the effective second-order nonlinearity (see Fig. 2), so that the maximum effective nonlinear coefficient is only $0.17d_{36}$. The coherent length for this media is only 23 μm that strongly reduces an efficiency of the second-harmonic generation. Nevertheless, the cascaded second-order

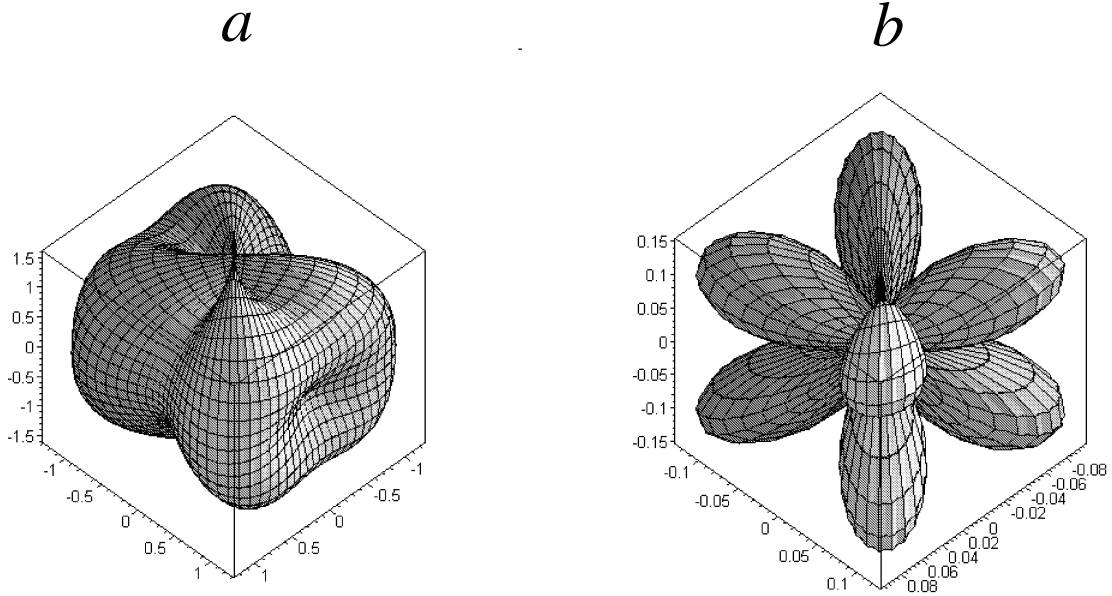


Figure 2. (a): Calculated orientational dependence of the third-order n_2 for ZnSe²⁰ scaled to $n_2^{[001]}$ and (b): orientational dependence of the second-order nonlinear coefficient scaled to its maximum value.

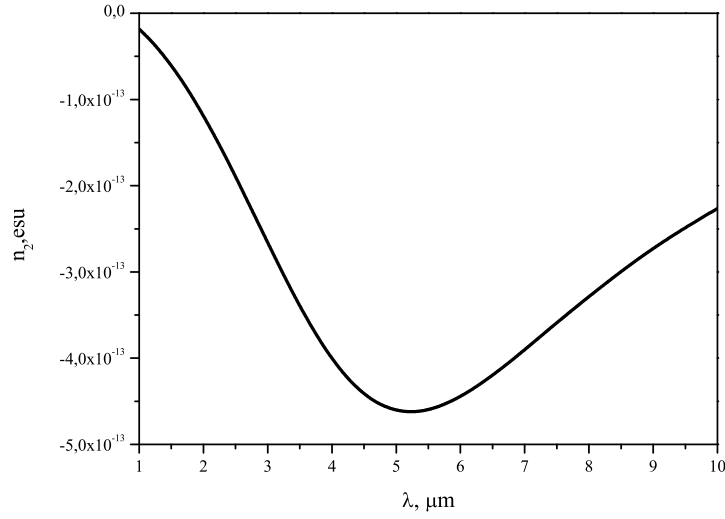


Figure 3. Calculated wavelength dependence of the cascaded n_2 for ZnSe.

process can contribute to the effective n_2 .^{21,22} Our calculation demonstrate (see Fig. 3¹⁹) that this contribution is small in the comparison with the third-order n_2 .

As a result, the simulation parameters corresponding to the above introduced normalizations are summarized in Table 2. $P = \sigma_a T_{cav} I_p / (\hbar \omega_0)$, $\epsilon = t_f E_s^{-1} / \delta$; $P_{cr} = 2n_0 / (n_2 k^2)$ and $I_{sat} = h\nu_0 / (\sigma_g T_r)$ are the critical power of the self-focusing (beyond the parabolical approximation for the Gaussian beam) and the gain saturation intensity,

respectively.

Table 2. Simulation parameters. $l_g=2\times 0.3$ cm, $T_{cav}=10$ ns, 2 W pump power, 100×100 μm^2 pump mode. We used the average value of n_2 and the minimum of T_r .

Medium	α_{max}	$n_2, 10^{-16}$ cm ² /W	P_{cr} , MW	$\delta, 10^{-12}$ cm ² /W	$\epsilon, 10^{-4}$	I_{sat} , kW/cm ²	t_f , fs	P, 10^{-3}
Cr:ZnSe	5	105	0.75	87	4.9	15	3.8	1.1
Cr:ZnS	5	42	1.5	32	10	28	3.7	0.62
Cr:ZnTe	5	178	0.52	314	3.8	13	4.5	1.9

3. DISTRIBUTED MODEL: RESULTS AND DISCUSSION

First of all we have to consider the meaning of the optimization procedure. The numerical simulations demonstrate that there exist some values of the saturation parameter σ , which provide the near chirp-free pulse generation. These values of σ can be considered as “optimal”. However, there is an additional factor, which has to be taken into account: the pulse shortening is possible by the σ growth and $\beta_2 \rightarrow 0$. We consider the values of β_2 and σ as optimal if they correspond to the generation of the shortest pulse. The main obstacle on the way of the pulse shortening is the multiple pulse generation.¹² The strong tendency to the multipulsing results from 1) E_s^{-1} decrease, 2) P increase, 3) fast absorber saturation favored by the large σ . The relatively large values of σ_g and λ_0 for the considered media result in the increase of the first parameter. However, the large absorption cross sections and SPM coefficients increase two later parameters. If the growth of the first parameter corresponds to the gain saturation and thereby to the stabilization of the pulse against the laser continuum growth, the larger P and σ initiate the rise of the continuum and the excitation of the perturbations inside the ultrashort pulse.²³ Hence, the optimization means the multiple pulses suppression allowing the pulse shortening.

Additional limitations on the pulse shortening result from the achievable values of the saturation parameter σ . In the KLM lasers this parameter is governed by the cavity alignment: the shift towards the cavity stability zone increases σ (see next section). So, the highest values of σ are reached in the immediate vicinity of the cavity stability boundary. This requires a too thorough cavity optimization and can not be considered as operational. Hence, the optimization aimed at the pulse shortening is based on the variation of all four parameters of master Eq. (1) and is constrained by the above described reasons.

Fig. 4 shows the parameters of Eq. (1), which for the fixed $\alpha - \rho$, γ and σ correspond to the minimum achievable β_2 , where the pulse width has a minimum. The further β_2 decrease results in the multipulse operation. Thus, the points in Fig. 4 lie on the boundary of the stable single pulse operation. There is a set of the general tendencies characterizing this boundary.

There exists a limited on $\alpha - \rho$ range of the stable single pulse operation, which expands as a result of the σ and γ growth. The increase of σ shifts this region towards the smaller $\alpha - \rho$. However, when $\sigma > 100$ the transition to multipulsing is possible. As every point in Fig. 4 corresponds to the fixed dimensionless E (see Fig. 5), the choice of the appropriate level of $\alpha - \rho$ for the fixed laser configuration (i.e. fixed γ , σ and β_2) is realized by the variation of P (pump, see Eq. (3)) as well as ρ (output loss). It is possible also to change α by the change of α_{max} due to variation of the crystal length or the active ions concentration or by the change of T_r due to variation of the active ions concentration. Note also, that the l_g decrease increases ϵ (due to the δ decrease), which describes the “strength” of the gain saturation relatively the SPM. Hence, ϵ increase expands the stability region towards the higher pump and allows the higher pulse energies (because they $\propto 1/\delta$).

The E decrease for the fixed $\alpha - \rho$, which takes a place for $\beta_2 \rightarrow 0$ (Fig. 5), has to be accompanied by P , α_{max} , T_r decrease or by ϵ , ρ increase in order to prevent from the continuum amplification. The last is the main source of the pulse destabilization and suppresses the single pulse operation in the vicinity of zero GDD. Hence, the pulse generation for $\alpha - \rho - \gamma > 0$ is not possible. $\alpha - \rho - \gamma = 0$ corresponds to the specific hybrid regime with the coexistent pulse and continuum.²⁴

Since the approach of the GDD to zero has to be accompanied by the pump decrease, this results in the growth of the σ required for the pulse stabilization (Fig. 4). This can demand too thorough cavity alignment. Moreover,

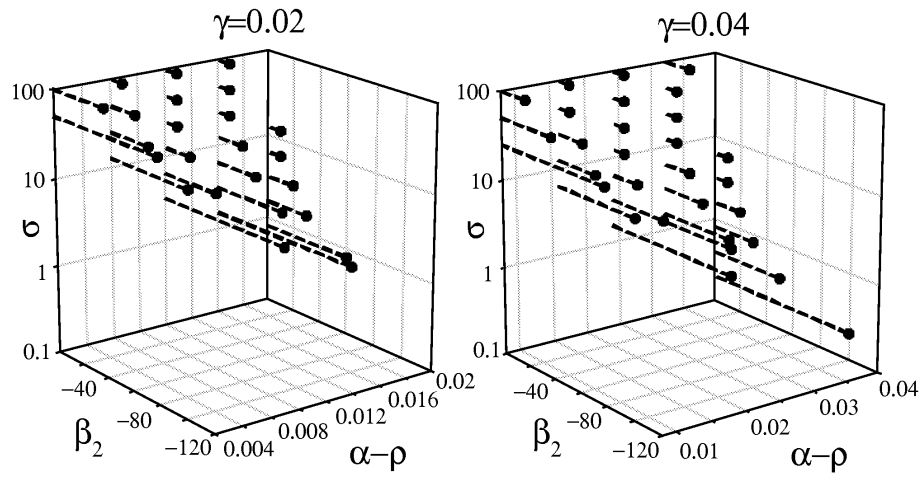


Figure 4. Stability boundary for the single pulse operation. Dimensional GDD [fs²] = $\beta_2 \times t_f^2$

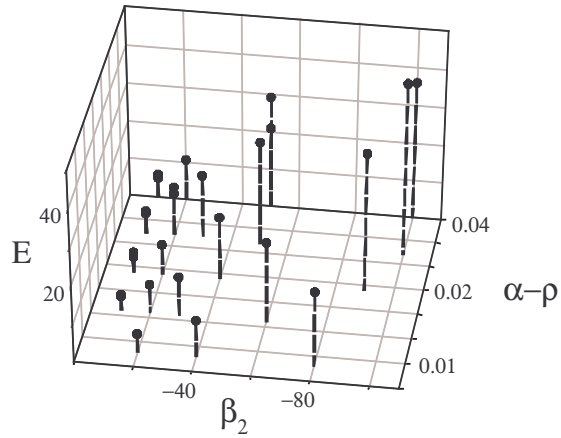


Figure 5. Pulse energy E on the stability boundary for $\gamma=0.04$.

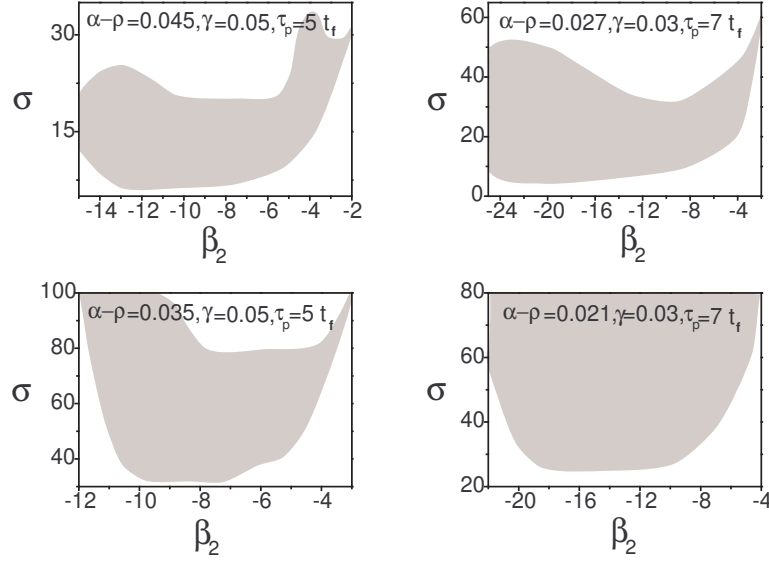


Figure 6. Regions of the σ and β_2 parameters providing the shortest pulses.

for the large σ we need the larger minimum $|\beta_2|$ providing the single pulse operation so that the dependence of the minimum $|\beta_2|$ on the σ for the fixed $\alpha - \rho$ has a parabolic-like form.²³

The most interesting features are the shift of the stability region towards the smaller σ (Fig. 4) and the pulse shortening as a result of the γ increase. For example, the minimum pulse duration τ_p for $\gamma = 0.03$ is $7t_f$ whereas for $\gamma = 0.05$ it is $5t_f$ (this is 19 fs for Cr:ZnSe and Cr:ZnS and 23 fs for Cr:ZnTe). The bad news here is the need for the hard-aperture KLM to provide the larger modulation depth. This reduces the KLM self-starting ability.

The regions of the parameters allowing the shortest pulses are shown in Fig. 6. The $\alpha - \rho$ increase reduces the minimum σ parameter producing the shortest pulses. However, the region of their existence shortens on σ .

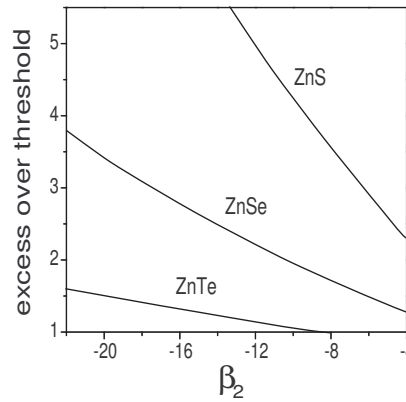


Figure 7. Pump threshold of KLM related to that for CW. Pulse duration is $\tau_p = 7t_f$. $\alpha = 0.071$, $\rho = 0.05$, $\gamma = 0.03$, $\alpha_{max} = 5$, other parameters correspond to Table 2.

Let us consider the concrete parameters of Table 2. The pump thresholds allowing $7t_f$ pulse durations are shown in Fig. 7. The threshold decreases from Cr:ZnS through Cr:ZnSe to Cr:ZnTe that results from the ϵ decrease. This

means that the SPM becomes stronger relatively the gain saturation under this transition. As a result, the tendency to the pulse destabilization intensifies and this demands to reduce the intracavity power by means of the pump decrease.

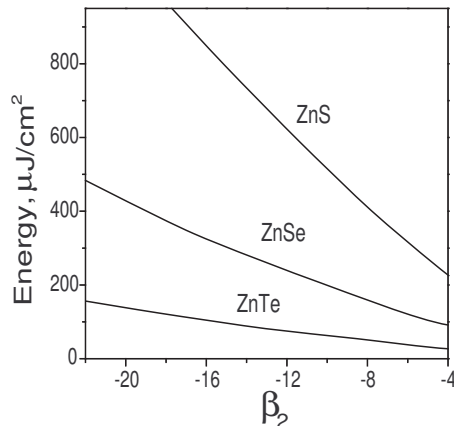


Figure 8. Intracavity pulse energy fluxes. The parameters correspond to Fig. 7.

Thus, the ϵ decrease reducing KLM threshold turns in the intracavity pulse energy decrease (Fig. 8). The highest value of ϵ for Cr:ZnS resulting from the large σ_g in the combination with comparatively small δ produces the stabilization of the shortest pulses with the highest energies.

Note, that the larger absorption cross-section for Cr:ZnTe results in the highest absorbed pump energy for the fixed pump intensity and mode area. This is a positive factor for the KLM threshold lowering. However, this can be a negative factor, when the SPM is the source of the pulse destabilization because the additional efforts for the intracavity power decrease are necessary (see also next section).

At last, we consider the contribution of the third-order dispersion, which can be large for the lasers under consideration. There are the technological troubles in the use of the chirped-mirror technique for the dispersion compensation in the mid-IR due to high value of λ_0 . Therefore the usual technique utilizing the prisms for the dispersion control can be useful in the considered situation. As a result, the third-order net-dispersion coefficient $|\beta_3|$ increases.

For the simulation we choose $\beta_3 = -5900 \text{ fs}^3$. As it can be seen from Fig. 9, the shape of the stability boundary does not change in the comparison to $\beta_3 = 0$.²⁵ However, the minimum pulse duration increases from $5t_f$ for $\beta_3 = 0$ to $9t_f$ (34 fs for Cr:ZnS, Cr:ZnSe and 40 fs for Cr:ZnTe). The additional effect is the pronounced (up to 140 nm) Stokes shift of the peak wavelength (Fig. 9 shows this shift on the stability boundary for Cr:ZnSe and Cr:ZnS). This shift is typical also for such IR lasers as Cr:LiSGaF, Cr:LiSAF, Cr⁴⁺:YAG^{16,25} and can reduce the pulse energy due worse overlap between gain band and pulse spectrum. However, for the media under consideration the wavelength shift is small in comparison with the full gain band width and the energy decrease is not critical.

4. TIME-SPATIAL MODEL: SELF-START ABILITY OF THE KERR-LENS MODE LOCKING

In the previous section we considered the ultrashort pulse stability on the basis of the distributed 1+1-dimensional model. However, this model can not provide answers to the basic questions: what is the self-start ability of the Kerr-lens mode locking and what has the real-world laser configuration to be?

These questions require an analysis on the basis of the time-spatial model. The simplest way is the assumption of the Gaussian spatial distribution for the laser beam reducing problem to the 1+2-dimensions. The free-space propagation of the Gaussian beam can be considered on the basis of the usual ABCD-matrix formalism, while the propagation inside the nonlinear active medium is described by the following equation:

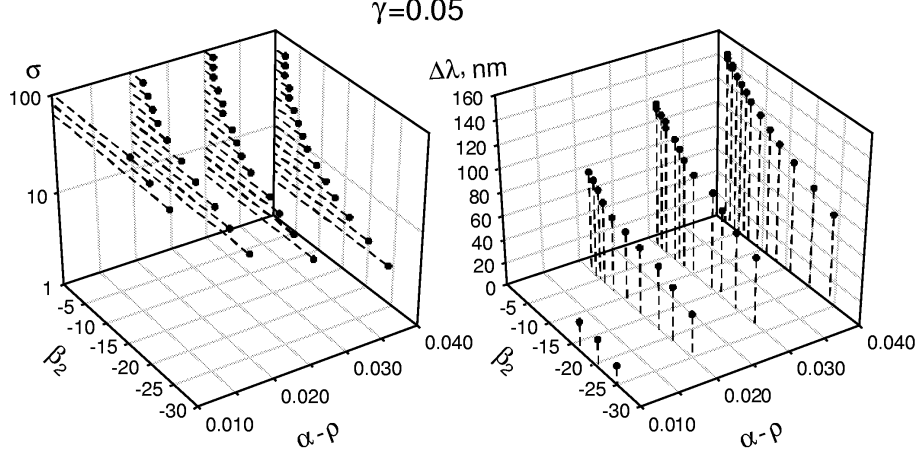


Figure 9. Stability boundary for the single pulse operation in the presence of the third-order dispersion and the Stokes spectral shift of the pulse spectrum on this boundary.

$$\frac{\partial a(z, r, t)}{\partial z} - i \left[\frac{2\vartheta r^2 a(z, r, t)}{w_p^2} - \frac{\frac{\partial a(z, r, t)}{\partial r} + \frac{r \partial^2 a(z, r, t)}{\partial r^2}}{2kr} + \beta_2' \frac{\partial^2 a(z, r, t)}{\partial t^2} \right] a(z, r, t) + i\chi |a(z, r, t)|^2 a(z, r, t) = \quad (5)$$

$$\alpha \exp\left(-\frac{2r^2}{w_p^2}\right) a(z, r, t) + t_f'^2 \frac{\partial^2 a(z, r, t)}{\partial t^2}.$$

Here β_2' and t_f' are the group-velocity dispersion and the inverse group-velocity delay coefficients (for ZnSe we used $\beta_2' = 2054 \text{ fs}^2/\text{cm}$ and $t_f' = 13 \text{ fs}/\text{cm}$).

The left-hand side of Eq. (5) describes the non-dissipative factors: thermo-lensing²⁶ ($\vartheta = k \frac{dn_0}{dT} \zeta P_a \exp(-\zeta z) / (4\pi n_0 \kappa_{th})$, k is the wave number, $\frac{dn_0}{dT}$ is the coefficient of the refractive index thermo-dependence ($5.35 \times 10^{-5} \text{ K}^{-1}$ for ZnSe), ζ is the loss coefficient at the pump wavelength, P_a is the pump power, κ_{th} is the thermo-conductivity coefficient ($0.172 \text{ W K}^{-1} \text{ cm}^{-1}$ for ZnSe)); diffraction (in the cylindrically symmetrical case); group-velocity dispersion and self-phase modulation (providing self-focusing for radially varying beam, $\chi = n_2 k / n_0$). The right-hand side of Eq. (5) describes the dissipative factors inside the gain medium: radially varying gain (providing gain guiding and soft aperture action, α and w_p are the saturated gain coefficient and the pump beam size, respectively); spectral filtering caused by the gain band profile.

It is convenient to rewrite Eq. (2) in the following way:

$$\alpha = \frac{2\alpha_{\max} \sigma_a P_a T_r}{\hbar \omega_p \pi w_p^2 \left(\frac{2\sigma_a P_a T_r}{\hbar \omega_p \pi w_p^2} + \frac{2v P_g \tau_p}{\pi w^2 I_s T_{cav}} + 1 \right)}, \quad (6)$$

where $v = E\pi w^2 / (2P_g \tau_p)$ (P_g is the generation power), w is the generation mode beam size. $v = \sqrt{\pi}/2$ for the pulse with the Gaussian time-profile, 2 for the *sech*-shaped pulse and 1 for the CW (in the latter case $\tau_p = T_{cav}$).

The crucial simplification in the analysis of Eq. (5) is based on the so-called aberrationless approximation: the propagating field has the invariable spatial-time profile, which is described by the set of the z -dependent parameters. In the non-dissipative case this approximation allows the variational approach providing rigorous description of the Gaussian beam propagation outside the parabolical approximation.^{27,28,29}

In the dissipative case we have to use the momentum method.³⁰ However, in contrast to Refs.^{31,32} we shall consider the momentums resulting from the symmetries of Eq. (5). The $a \rightarrow a \exp(i\phi)$ invariance, the transverse and time translating invariance suggest the following momentums³³:

$$\begin{aligned}
T_{m,n} &= \iint_{\infty} r^m t^n |a|^2 dr dt, \\
J_{m,n} &= \iint_{\infty} r^m t^n \left(a \frac{\partial a^*}{\partial t} - a^* \frac{\partial a}{\partial t} \right) dr dt, \\
M_{m,n} &= \iint_{\infty} r^m t^n \left(a \frac{\partial a^*}{\partial r} - a^* \frac{\partial a}{\partial r} \right) dr dt.
\end{aligned} \tag{7}$$

Like the variational approach we can substitute to Eqs. (4) the trial solution describing the ultrashort pulse. If we take the Gaussian time-spatial profile $a(z, r, t) = W(r) \exp\left(G(r) - \frac{r^2}{2w(r)^2} + ib(r)r^2 - \frac{t^2}{\tau(r)^2} + i\psi(r)t^2\right)$ ($W(r)$ is the complex amplitude, $2w'^2=w^2$, $G(r)$ is the pulse amplification parameter excepting the geometrical magnification for the Gaussian beam), the equations describing the evolution of the pulse and beam parameters are³⁴:

$$\begin{aligned}
\frac{dw'}{dz} &= -\frac{2}{k}w'(z)b(z) - \frac{2\alpha w'(z)^3}{w_p^2 \left(1 + \frac{2w'(z)^2}{w_p^2}\right)^{3/2}}, \\
\frac{d\tau(z)}{dz} &= \left[\frac{2}{\tau(z)} - 2\tau(z)^3 \psi(z)^2 \right] t_f^2 + 2\beta_2'^2 \tau(z) \psi(z), \\
\frac{dG(z)}{dz} &= \frac{\alpha}{1 + \frac{2w'(z)^2}{w_p^2}} - \frac{2t_f^2}{\tau(z)^2} - \beta_2'^2 \psi(z), \\
\frac{db(z)}{dz} &= \frac{2\vartheta}{w_p^2} + \frac{2b(z)^2}{k} + \frac{\sqrt{2}P_0 e^{2G(z)}}{\pi P_{cr} k w(z)^4} - \frac{1}{2kw'(z)^4}, \\
\frac{d\psi(z)}{dz} &= 2\beta_2'^2 \left(\frac{1}{\tau(z)^4} - \psi(z)^2 \right) - \frac{8t_f^2 \psi(z)}{\tau(z)^2} + \frac{2P_0 e^{2G(z)}}{\pi P_{cr} w(z)^2 \tau(z)^2}, \\
P_g &= P_0 e^{2G(z)},
\end{aligned} \tag{8}$$

where P_0 and w'_0 are the power and the beam size before the active medium, respectively.

Eq. (8) in the combination with the ABCD-formalism allows defining the stability regions for CW, single- and multiple pulsing (the latter requires the trivial generalization of the trial function). Such regions can predict the real-world laser configurations providing the self-starting Kerr-lens mode locking.

As it is seen from Table 2 the main features of the considered active media are the comparatively low P_{cr} (e.g. $P_{cr}=2.6$ MW for Ti:sapphire) and the extremely low I_{sat} (300 kW for Ti:sapphire). This causes the stabilization of the CW against the mode locking due to the strong gain saturation. However, as it is seen from Eqs. (6, 8) (note that the gain saturation is intensity-dependent, but the self-focusing is power-dependent), we can enhance the tendency to the mode locking due to the suppression of the gain saturation. This can be achieved by the growth of the generation mode within the active medium owing to, for example, the cavity shortening or the decrease of the folding mirrors curvature (Fig. 10). At the same time we have to keep the moderate level of the absorbed pump power and to use the asymmetrical cavity in order to separate the stability zones. The preferable configurations correspond to the pulse operation without the CW. This occurs between the CW stability zones (see Fig. 10).

5. CONCLUSION

In conclusion, we presented the models, which can be usable for the numerical optimization of the KLM lasers. On the basis of these models, the KLM abilities of the Cr-doped Zinc-chalcogenides were estimated. It was shown, that the strong SPM inherent to these media and destabilizing the single pulse operation can be overcome by the choice of the appropriate GDD, pump, modulation depth and saturation parameter of the Kerr-lensing induced fast

saturable absorber. As a result, the Cr:ZnTe possesses the lowest KLM threshold, however strong SPM constrains the achievable pulse power for this laser. The best stability for the highest energy flux and the shortest pulse duration (19 fs) are achievable in Cr:ZnS, Cr:ZnSe. The presence of the third-order dispersion increases the minimum achievable pulse durations up to 34 - 40 fs and causes the strong (up to 140 nm) Stokes shift of the generation wavelength. However, the latter effect does not reduce noticeably the pulse energy. The Kerr-lens mode locking self-start ability of the considered active media is reduced by the strong gain saturation so that the cavity tuning providing the ultrashort pulsing differs essentially from that for the Ti:sapphire. We have to avoid over-pumping and over-shortening of the generation mode. As a result, the short and asymmetrical cavities with the comparatively large curvature of the folding mirrors are preferable. On the whole, the Cr-doped Zinc-chalcogenides have the prospects for the sub-50 fs generation that amounts to only few optical cycles around 2.5 μm .

ACKNOWLEDGMENTS

This work was supported by Austrian National Science Fund Project M688.

REFERENCES

1. L.D.DeLoach, R.H.Page, G.D.Wilke, S.A.Payne, and W.F.Krupke. "Transition metal-doped Zinc chalcogenides: spectroscopy and laser demonstration of a new class of gain media," *IEEE J. Quantum Electron.* **32**, pp. 885–895, 1996.
2. R.H.Page, K.I.Schaffers, L.D.DeLoach, G.D.Wilke, F.D.Patel, J.B.Tassano, S.A.Payne, W.F.Krupke, K.-T.Chen, A.Burger. "Cr²⁺:doped Zinc chalcogenides as efficient widely tunable mid-infrared lasers," *IEEE J. Quantum Electron.* **33**, pp. 609–619, 1997.
3. U.Hömmrich, X.Wu, V.D.Davis, S.B.Trivedi, K.Grasze, R.J.Chen, S.W.Kutcher. "Demonstration of room-temperature laser action at 2.5 μm from Cr²⁺:Cd_{0.85}Mn_{0.15}Te," *Optics Lett.* **22**, pp. 1180–1182, 1997.
4. J.McKay, K.L.Schepler, G.C.Catella. "Efficient grating-tuned mid-infrared Cr²⁺:CdSe laser," *Optics Lett.* **24**, pp. 1575–1577, 1999.
5. G.J.Wagner, T.J.Carrig. "Power scaling of Cr²⁺:ZnSe lasers," in *OSA Trends in Optics and Photonics*, vol. 50, *Advanced Solid-State Lasers*, Cr. Marshall, ed. (OSA, Washington DC 2001), pp. 506–510.
6. I.T.Sorokina, E.Sorokin, A.DiLieto, M.Tonelli, R.H.Page. "Tunable diode-pumped continuous-wave operation and passive mode-locking of Cr²⁺:ZnSe laser," in *Conference on Lasers and Electro-Optics/Europe 2001*, Conference Digest, Munich, p. 151, 2001.
7. E.Sorokin, I.T.Sorokina. "Tunable diode-pumped continuous-wave Cr²⁺:ZnSe laser," *Applied Physics Lett.*, **80**, pp. 3289–3291, 2002.
8. T.J.Carrig, G.J.Wagner, A.Sennaroglu, J.Y.Jeong, C.R.Pollock. "Mode-locked Cr²⁺:ZnSe laser", *Optics Lett.*, **25**, pp. 168–170, 2000.
9. E.Sorokin, I.T.Sorokina, R.H.Page. "Room-temperature CW diode-pumped Cr²⁺:ZnSe laser", in *OSA Trends in Optics and Photonics*, vol. 50, *Advanced Solid-State Lasers*, Cr. Marshall, ed. (OSA, Washington DC 2001), pp. 101–105.
10. K.Graham, S.Mirov, V.Fedorov, M.E.Zvanut, A.Avanesov, V.Badikov, B.Ignat'ev, V.Panutin, G.Shevirnyaeva. "Spectroscopic characteristics and laser performance of diffusion doped Cr²⁺:ZnS," in *OSA Trends in Optics and Photonics*, vol. 50, *Advanced Solid-State Lasers*, Cr. Marshall, ed. (OSA, Washington DC 2001), pp. 561–567.
11. I.T.Sorokina, E.Sorokin, S.Mirov, V.Fedorov, V.Badikov, V.Panyutin, K.I.Schaffers. "Broadly tunable compact continuous-wave Cr²⁺:ZnS laser," *Optics Lett.*, **27**, pp. 1040–1042, 2002.
12. V.L.Kalashnikov, E.Sorokin, I.T.Sorokina. "Multipulse operation and limits of the Kerr-lens mode locking stability for Cr²⁺:ZnSe laser," in *OSA Trends in Optics and Photonics*, vol. 65, *Advanced Solid-State Lasers*, M.E. Fermann, L.R. Marshall, eds. (OSA, Washington DC 2002), pp. 374–378.
13. V.P.Kalosha, M.Müller, J.Herrmann, and S.Gatz. "Spatiotemporal model of femtosecond pulse generation in Kerr-lens mode-locked solid-state lasers", *J. Opt. Soc. Am. B*, **15**, pp. 535-550, 1998.
14. I.S.Aranson, L.Kramer. "The world of the complex Ginzburg-Landau equation", *Rev. Modern Physics*, **74**, pp. 99-143, 2002.
15. H.A.Haus, J.G.Fujimoto, E.P.Ippen. "Analytic theory of additive pulse and Kerr lens mode locking", *IEEE J. Quantum Electron.* **28**, pp. 2086–2096, 1992.

16. V.L.Kalashnikov, E.Sorokin, I.T.Sorokina. "Mechanisms of spectral shift in ultrashort-pulse laser oscillators", *J. Opt. Soc. Am. B* **18**, pp. 1732–1741, 2001.
17. M.Sheik-Bahae, D.C.Hutchings, D.J.Hagan, E.W.van Stryland. "Dispersion of bound electronic nonlinear refraction in solids", *IEEE J. Quantum Electron.* **27**, pp. 1296–1309, 1991.
18. D.C.Hutchings, B.S.Wherrett, "Theory of the dispersion of ultrafast nonlinear refraction in zinc-blende semiconductors below the band edge", *Phys. Rev. B* **50**, pp. 4622–4630, 1994.
19. see on-line <http://www.geocities.com/optomaplev/programs/znse.html>
20. D.C.Hutchings, B.S.Wherrett, "Theory of the anisotropy of ultrafast nonlinear refraction in zinc-blende semiconductors", *Phys. Rev. B* **52**, pp. 8150–8159, 1995.
21. R.L.Sutherland, *Handbook of nonlinear optics*, New York (1996), p.323
22. R.Schiek,"Nonlinear refraction caused by cascaded second-order nonlinearity in optical waveguide structures", *J. Opt. Soc. Am. B* **10**, pp. 1848–1855, 1993.
23. V.L.Kalashnikov, E.Sorokin, I.T.Sorokina. "Multipulse operation and limits of the Kerr-lens mode locking stability", *IEEE J. Quantum Electron.* **39**, pp. 323–336, 2003.
24. N.N.Akhmediev, V.V.Afanasjev, J.M.Soto-Crespo. "Singularities and special solutions of the cubic-quintic complex Ginzburg-Landau equation," *Phys. Rev. E*, **53**, pp. 1190–1201, 1996.
25. detailed investigations show some interesting modification of the single pulse stability and its spectral characteristics, see V.L. Kalashnikov, S. Naumov, E. Sorokin, I. Sorokina, "Spectral broadening and shift of the few optical cycle pulses in Cr⁴⁺:YAG laser," in Program of ASSP'2003, San Antonio, USA, February 2-5, TuB1, 2003.
26. M.Mehendale, T.R.Nelson, F.G.Omenetto, W.A.Schroeder. "Thermal effects in laser pumped Kerr-lens mode-locked Ti:sapphire lasers", *Optics Commun.* **136**, pp. 150–159, 1997.
27. D.Anderson. "Variational approach to nonlinear pulse propagation in optical fibers", *Phys. Rev. A* **27**, p. 3135, 1983.
28. M.Karlsson, D.Anderson, M.Desaix, M.Lisak. "Dynamic effect of Kerr nonlinearity and spatial diffraction on self-phase modulation of optical pulses", *Optics Lett.* **16**, pp. 1373–1375, 1991.
29. M.Desaix, D.Anderson, M.Lisak. "Variational approach to collapse of optical pulses", *J. Opt. Soc. Am. B* **8**, p. 2082–2086, 1991.
30. S.N.Vlasov, V.A.Petrishchev, V.I.Talanov. "Averaged description of wave beams in linear and nonlinear media", *Izvestija vuzov (radiophysika)* **14**, p. 1353–1363, 1971 (in russian).
31. J.Herrmann. "Theory of Kerr-lens mode locking: role of self-focusing and radially varying gain", *J. Opt. Soc. Am. B* **11**, pp. 498–512, 1994.
32. V.P.Kaloshia, M.Mueller, J.Herrmann, S.Gatz. *J. Opt. Soc. Am. B* **15**, p. 535–550, 1998.
33. N.N.Akhmediev, A.Ankiewicz, *Solitons: Nonlinear Pulses and Beams* (Chapman&Hall, London, 1997).
34. on-line <http://www.geocities.com/optomaplev/programs/selfff.html>

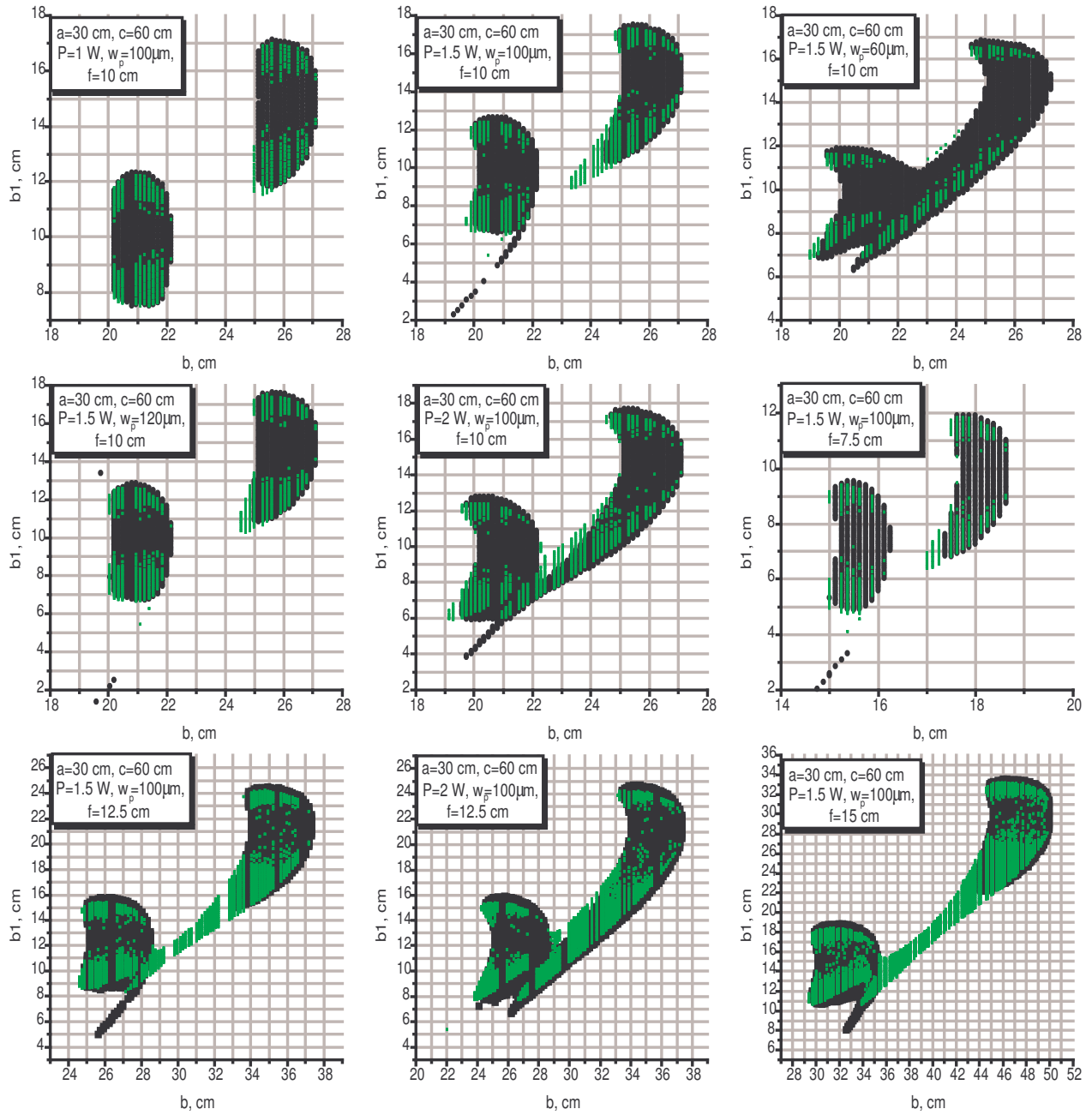


Figure 10. Stability ranges for the CW (black filled circles) and mode locking (open green circles). a and c are the cavity arms, b is the folding distance, b_1 is the distance of the active medium facet from the curved mirror forming the shorter cavity arm, f is the focal length of the curved mirrors. $\rho=0.05$.